THE ASTROPHYSICAL JOURNAL, 571:L181–L185, 2002 June 1

LARGE-SCALE SOLAR CORONAL STRUCTURES IN SOFT X-RAYS AND THEIR RELATIONSHIP TO THE MAGNETIC FLUX

E. E. BENEVOLENSKAYA,[1,2] A. G. KOSOVICHEV,[1] J. R. LEMEN,[3] P. H. SCHERRER,[1] AND G. L. SLATER[3]
Received 2002 January 19; accepted 2002 April 15; published 2002 May 6

ABSTRACT

We have investigated the relationship between magnetic activity and coronal structures using soft X-ray data from the *Yohkoh* soft X-ray telescope and magnetic field data from the Kitt Peak Solar Observatory for the period of 1991–2001 and EUV data from the *Solar and Heliospheric Observatory* EUV Imaging Telescope for 1996–2001. The data are reduced to Carrington synoptic maps, which reveal two types of migrating structures of coronal activity at low and high latitudes in the time-latitudinal distribution. The low-latitude coronal structures, migrating equatorward, correspond to photospheric sunspot activity, and the high-latitude structures migrating toward the poles reflect polar activity of the Sun. We present the following new results:

1. The migrating high-latitude coronal magnetic structures are revealed in the soft X-ray data as complete bright giant loops connecting the magnetic field of the following part of active regions with the polar field. They appear during the rising phase and maximum of the solar cycle and show quasi-periodic impulsive variations with a 1–1.5 yr period.
2. The soft X-ray intensity of these loops has a strong power-law correlation with the photospheric magnetic flux. The power-law index, which on average is close to 2, shows variations with the solar cycle: it is higher for the period of the declining phase and minimum of solar activity than for the rising phase and maximum.

Subject headings: Sun: activity — Sun: corona — Sun: magnetic fields — Sun: UV radiation — Sun: X-rays, gamma rays

1. INTRODUCTION

Large-scale coronal structures play a very important role in understanding the topological evolution of the solar magnetic field during the solar cycle. They have a long history of investigation since Secchi (1877) discovered the migration of the zone of polar prominences poleward during the rising phase of the solar cycle. There are two types of structures in coronal emission at low and high latitudes migrating equatorward and poleward, respectively, with the solar cycle. These structures, sometimes called "coronal activity waves," are thought to be related to dynamo waves, which describe latitudinal migration of magnetic zones (e.g., Makarov, Ruzmaikin, & Starchenko 1987; Belvedere, Lanzafame, & Proctor 1991).

Recently, we have identified the two types of coronal activity waves in the extreme ultraviolet data from the *Solar and Heliospheric Observatory* (*SOHO*) EUV Imaging Telescope (EIT; Benevolenskaya, Kosovichev, & Scherrer 2001). It was found that the bright high-latitude coronal structures, which migrate to the poles during the rising phase of the solar cycle, are formed by density enhancements in the poleward footpoints of magnetic field lines. These magnetic lines connect the magnetic fields of the following parts of active regions with the polar field and are represented by giant polar coronal loops. These giant magnetic loops connect the toroidal field of the new solar cycle with the polar poloidal field formed during the previous cycle. In this Letter, we extend the analysis by using observations of the solar corona during 1991–2001 in soft X-rays from the soft X-ray telescope (SXT) on *Yohkoh* (Tsuneta et al. 1991). This period covers the declining phase of solar cycle 22 and the rising phase of the current cycle, 23.

2. DATA ANALYSIS

The image sets (from which the SXT synoptic maps were derived) consist of full-Sun images taken in two different filters of the *Yohkoh* SXT: a thin Al filter with an approximate passband of ≈6–13 Å (Al) and a composite Al/Mg/Mn filter with a slightly shorter passband of ≈5–12 Å (AlMg) from 1991 November 11 to 2001 March 13. The full SXT image archive contains images taken at different resolutions (2.″45, 4.″91, and 9.″8). Full-disk images were chosen at a 6 hr cadence at the highest resolution available at each sample time. Most of the images are 4.″91 resolution images. Each raw image was processed in the following way: The instrumental background noise was subtracted. In addition, contamination from white-light leakage onto the CCD was subtracted using a sophisticated model of the instrumental white-light leakage pattern. The instrumental point-spread scattering response of the mirror and vignetting effects were removed by deconvolution. Finally, regions of the image where CCD saturation had occurred (at the bright cores of active regions) were corrected by an image compositing algorithm that uses an independent but nearly simultaneous short-exposure image. The SXT measurements are represented in terms of "data numbers" (DNs). The conversion to the energy flux depends on a temperature model of the solar corona, which is currently uncertain. Under a commonly used fixed-temperature approximation, the energy flux is proportional to DN (e.g., Wolfson et al. 2000).

The Carrington synoptic maps of the corona are represented by values of the intensity centered on the central meridian. The resolution of these maps is 1° in both longitude from 0° to 360° and latitude from −83° to 83°. To obtain the latitudinal distribution, we averaged the synoptic maps over longitude and plotted as a function of latitude and time.

[1] W. W. Hansen Experimental Physics Laboratory, Stanford University, Stanford, CA 94305-4085.
[2] Pulkovo Astronomical Observatory, St. Petersburg 196140, Russia.
[3] Lockheed Martin Solar and Astrophysics Laboratory, 3251 Hanover Street, Palo Alto, CA 94304.

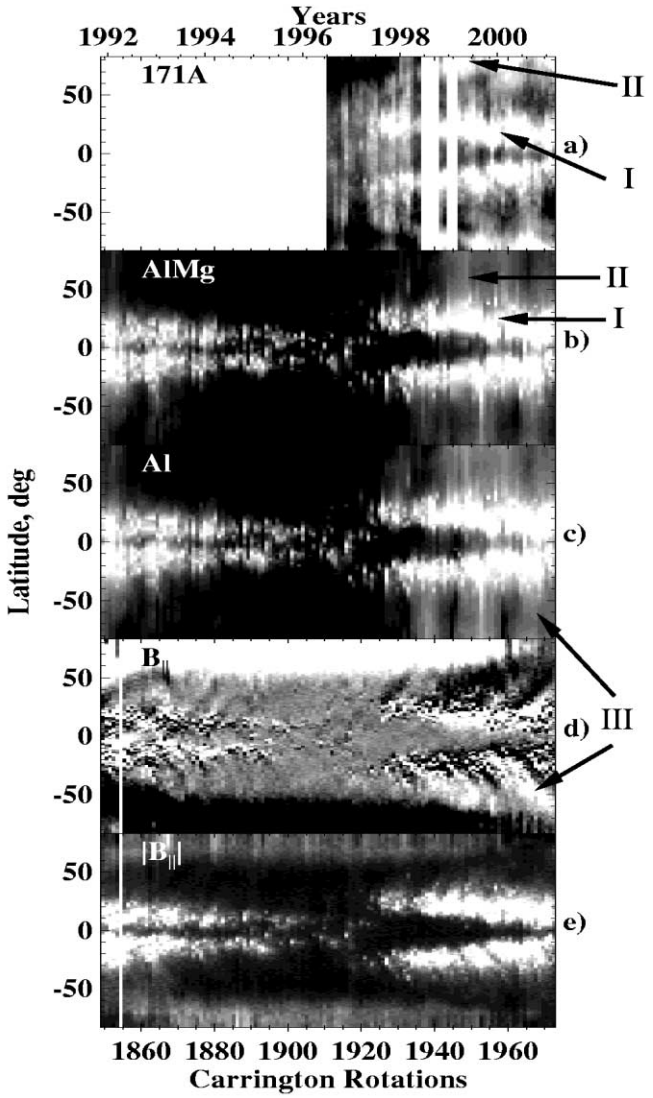

FIG. 1.—Axisymmetrical distributions as a function of latitude (from −83° to 83°) and time from 1991 November 11 to 2001 March 13 (CR 1849–1973) for (*a*) EUV flux in Fe IX, X lines (available only since CR 1911, 1996 June 28), (*b*) X-ray flux in the AlMg filter, (*c*) X-ray flux in the Al filter, (*d*) $B_{\|}$-component of the magnetic field, where the gray-scale range is [−1 G, 1 G], and (*e*) unsigned magnetic flux $|B_{\|}|$, in the [0 G, 10 G] range.

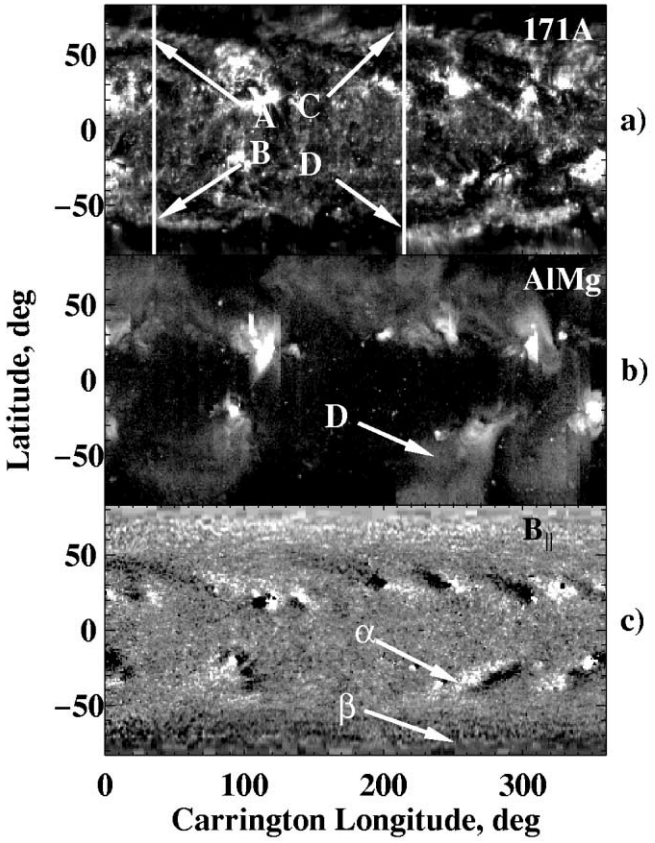

FIG. 2.—Synoptic maps for CR 1929 (1997 November 1–28). (*a*) Logarithm of the EUV intensity in Fe IX, X lines in the range [3.8, 7]; (*b*) log intensity of the X-ray flux in the AlMg filter in the range [0, 6]. (*c*) $B_{\|}$-component of the magnetic field, [−20 G, 20 G]. Vertical lines indicate the position of the solar limb of the EIT image of 1997 November 19, shown in Figs. 3*a* and 3*b*, and A, B, C, and D indicate coronal structures corresponding to the giant polar loops in Fig. 3*a*. Arrows in the magnetic map show the regions of the positive polarity, α (the following part of an active region), and the negative polarity, β (the polar field), which are connected by loop D.

Examples of the latitudinal distribution of the EUV and soft X-ray intensity are shown in Figures 1*a*–1*c*. For comparison, in Figures 1*d* and 1*e*, we plot the azimuthally averaged distributions of the line-of-sight magnetic flux, $B_{\|}$, and the corresponding unsigned (absolute) magnetic flux, $|B_{\|}|$, obtained from the Kitt Peak Observatory synoptic magnetic maps. The zonal magnetic neutral lines separating magnetic polarities at high latitudes are seen as contrast lines between white and dark colors in Figure 1*d*. These neutral lines reflect the position of $B_{\|} = 0$ for magnetic field averaged over longitude and separating the polar field formed during the previous solar cycle from the field that emerged during the current cycle. The mean locations of these lines in both hemispheres progressively migrates toward the poles. When the neutral lines reach the poles (usually around the sunspot maxima), this corresponds to magnetic polarity reversal at the poles. The $|B_{\|}|$ map, which shows the location active regions, reveals the usual "butterfly" diagram.

3. CORONAL ACTIVITY STRUCTURES

The coronal EUV map (Fig. 1*a*) shows in each hemisphere two sets of migrating structures: low-latitude structures (labeled I) that migrate toward the equator following the evolution of $|B_{\|}|$ (low-latitude coronal activity waves) and high-latitude structures (II), or high-latitude waves, that migrate toward the poles parallel to the magnetic neutral lines. In the SXT coronal maps (Figs. 1*b* and 1*c*), the low-latitude migrating structures are similar to those in the EUV map. However, the high-latitude structures look different, without pronounced brightening in the polar regions and more uniform latitudinally, connecting the low-latitude bands with the polar regions. These high-latitude structures appear mostly during the rising phase of the solar cycle.

In the individual EUV synoptic maps, the high-latitude structures are easily identified as longitudinally extended bright structures at 50°–83° latitude, labeled A–D in Figure 2*a*. In the corresponding SXT maps, they represent diffuse structures extended in latitude from $\sim \pm 30°$ to the polar boundaries of our maps at $\pm 83°$ (e.g., feature D in Fig. 2*b*).

The comparison between the high-latitude coronal structures and the photospheric magnetic field (Fig. 2*c*) shows that these structures represent giant loops connecting the polar poloidal magnetic field formed during the preceding cycle and the to-

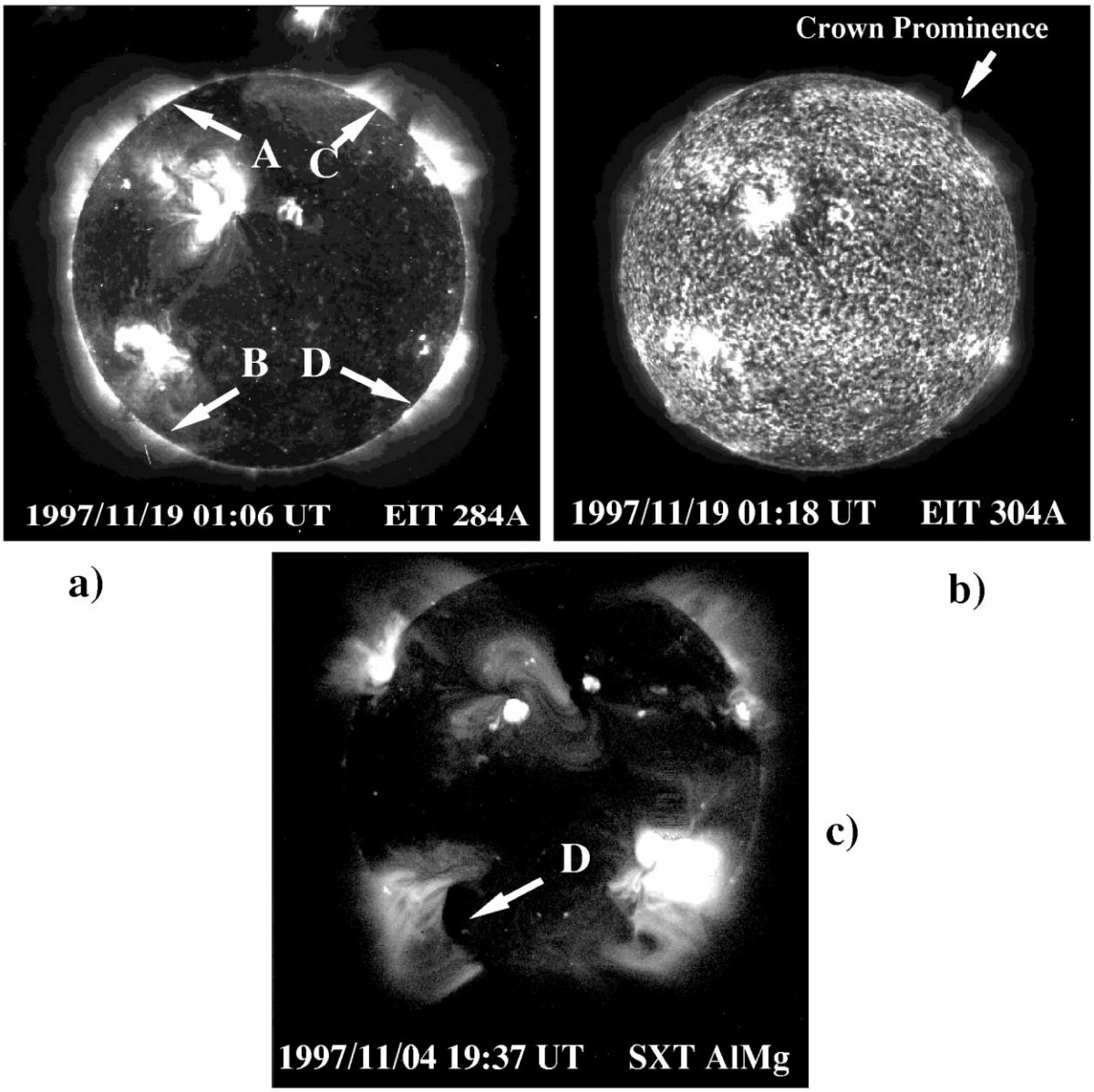

FIG. 3.—(*a*) EUV/EIT image in the Fe XV line. The arrows identify footpoints of the giant loops (A–D) that are parts of the longitudinally extended high-latitude structures indicated in Fig. 2*a*. (*b*) EUV/EIT image in the He II line. The arrow indicates a crown polar prominence that was located inside the giant loop on the west limb. (*c*) X-ray image in the AlMg filter showing the giant loop D on the disk.

roidal field of the new cycle. In EUV, we mostly see the poleward footpoints of these structures, while in the SXT data we see the whole giant loop structures on the disk. On the solar limb, these structures are seen in EUV as footpoints of the giant loops and sometimes as whole giant loops connecting the following parts of the active regions with the polar regions (Fig. 3*a*). Quite often, these loops have low-altitude dark structures in the middle, which correspond to polar crown prominences (Fig. 3*b*). These polar giant loops are clearly seen in SXT data on the solar disk (e.g., feature D in Fig. 3*c*).

The axisymmetrical distributions of the coronal intensity shown in Figure 1 also reveal that the high-latitude coronal structures (visible as bright connections between the low-latitude coronal structures and polar regions) tend to appear quasi-periodically with ~1–1.5 yr period, correlating with "impulses" of magnetic flux. An example of such impulse in the soft X-ray and magnetic fluxes is indicated by arrows and "III" in Figures 1*c* and 1*d*.

Figure 4 shows the variations with time of the X-ray and EUV intensities in the latitudinal zones between 50° and 70° in both hemispheres. Apparently, these impulses appear in the northern and southern hemispheres almost in antiphase. They correlate with variations of the magnetic flux at lower latitudes, 25°–35°, shown by dotted curves in Figure 4. This correlation, which was also found by Wolfson et al. (2000), is particularly prominent in the north (Fig. 4*b*).

4. RELATIONSHIP BETWEEN THE CORONAL X-RAY INTENSITY AND MAGNETIC FLUX DURING THE DECLINING AND RISING PHASES OF THE SOLAR CYCLE

Using the axisymmetrical distributions presented in Figure 1, we have investigated the relationship between the soft X-ray emission and the magnetic flux in the low- and midlatitude zone from −55° to 55°. Figures 5*a* and 5*b* show the scatter plots of intensity of SXT data in the AlMg filter as a function of the

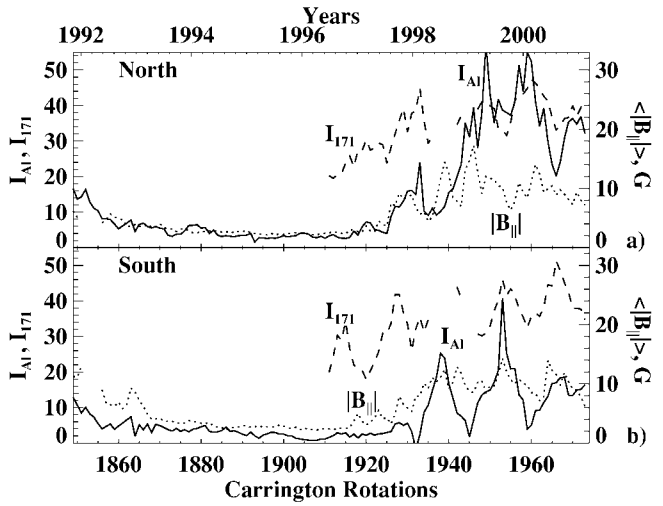

FIG. 4.—Variation of soft X-ray intensity, I_{A1} (*solid curve*), and the EUV intensity, I_{171} (*dashed curve*), averaged in the high-latitude zones from 50° to 70°, and the mean magnetic flux, $\langle |B_{||}| \rangle$, in the low-latitude zone, 25°–35°, in the (*a*) northern and (*b*) southern hemispheres as a function of Carrington rotation number and time.

unsigned magnetic flux (from Kitt Peak Observatory) separately for the declining and rising phases of the solar cycle. The data are divided into 12 groups of 10 Carrington rotations (except the first and last groups, which consist of three and 13 rotations) and are represented by different colors for each group. The separate scatter plots for each of the 12 groups of data are presented by Benevolenskaya et al. (2002).

We find a good correlation between the intensity of the soft X-ray emission and the magnetic flux with the correlation coefficient $r \simeq 0.9$. On the first sight, we see two different dependences of $\log I_{\rm AlMg}(\log |B_{||}|)$ when $\log |B_{||}| < 1.5$ and $\log |B_{||}| > 1.5$ (8 G) in these distributions. In the weaker magnetic flux range, the dependence is significantly steeper than for the stronger flux. This apparent steep change in the scatter plots occurred partly because of the changes of the mean level of X-ray intensity during the low-activity phases of the solar cycle. The evolution of the level of the X-ray intensity can be tracked by looking at stacks of the different color points in Figures 5*a* and 5*b*.

It is emphasized by Sturrock (1999) that the relationship between the energy flux into the corona (F) and the magnetic flux at the photospheric level is most likely represented by the power law $F \sim \langle |B| \rangle^n$. Soft X-ray measurements are used as a proxy for energy flux. We have found that the power-law index calculated by a straight-line least-squares fit to all points in Figures 5*a* and 5*b* is approximately the same for the two periods, 2.03 ± 0.01 and 1.98 ± 0.01. However, for the higher magnetic flux range ($\log |B_{||}| > 1.5$), the power-law index is significantly different: 1.85 ± 0.02 for CR 1849–1911 (the period of declining activity) and 1.64 ± 0.02 for CR 1911–1973 (the period of rising activity).

We have also calculated the power-law index for the individual 12 subintervals of the 10 rotations indicated in Figure 5, using the whole magnetic flux range. The results shown in Figure 6 indicate that the power index varies with the solar cycle between 1.5 in the solar maximum and 2.2 in the minimum. This suggests that the soft X-ray flux depends not only on the amount of the photospheric magnetic flux but, perhaps, also on some magnetic field structural properties that vary with the solar cycle.

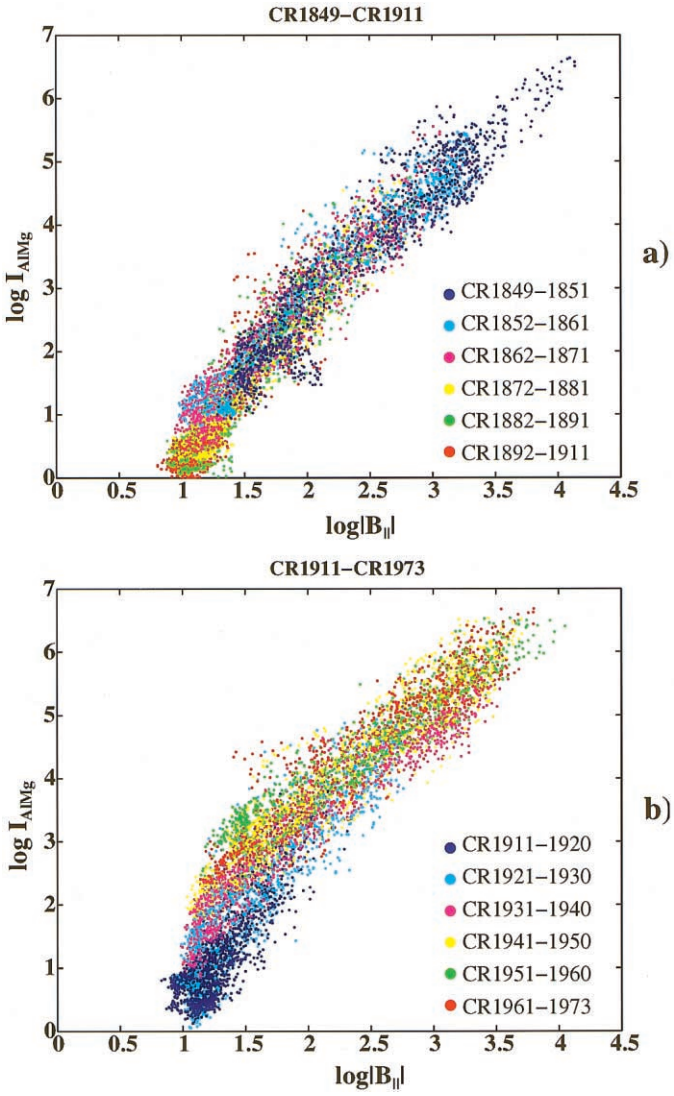

FIG. 5.—Scatter plots of the soft X-ray intensity from SXT (*Yohkoh*) data in the AlMg filter as a function of the magnetic flux (from Kitt Peak Observatory) in the natural logarithmic scale for the latitudinal zone from −55° to 55° for two periods: (*a*) 1991 November 11 to 1996 July 25 and (*b*) 1996 June 28 to 2001 March 13. Different subperiods are marked by different colors. The color-coding in terms of Carrington rotation numbers is shown in the figures.

5. DISCUSSION

The results of our analysis of 10 yr of coronal and magnetic data lead to several conclusions that are important for understanding the evolution of the solar corona with the activity cycle. The migrating poleward high-latitude coronal structures (coronal activity waves) that received significant attention in the past and that are represented by the bright polar footpoints of the giant loops in the EUV/EIT data are visible as the whole loop structures on the solar disk in the soft X-ray *Yohkoh*/SXT data. Therefore, the temperature of these loops is in the range of (2–3) × 10^6 K. The giant magnetic loops connect the magnetic flux of the following parts of the active regions with the magnetic flux of the polar regions that have the opposite polarity.

The giant loops are most likely formed by magnetic reconnections in the corona and provide an important topological connection between the poloidal magnetic field formed during the previous solar cycle in the polar regions with the toroidal

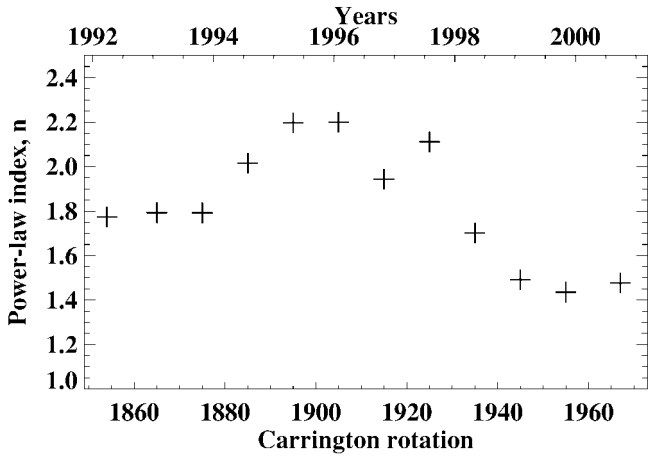

FIG. 6.—Power-law index, n, of the $I_{\mathrm{AlMg}} \sim \langle |B_{\parallel}| \rangle^{n}$ dependence as a function of Carrington rotation number and time.

low-latitude field of the new cycle. The *Yohkoh* data show that these large-scale magnetic connections appear mostly during the rising phase of the solar cycle and its maximum. These connections did not appear or were very weak during the declining phase of the solar cycle. The high-latitude coronal activity waves in the SXT data are closely related to the low-latitude magnetic flux and sunspot numbers and display intriguing quasi-periodic impulses with the characteristic period of 1–1.5 yr.

The low-latitude coronal structures show the butterfly-type distributions in both the EUV and SXT data and correlate with the photospheric magnetic flux in the same latitudinal zones. The relation between the soft X-ray flux, which is considered a proxy of the coronal energy flux, and the magnetic flux can be approximated by a power law with an averaged index close to 2. However, this relation changes with the solar cycle. During the solar maxima, the power-law index is lower than the average, about 1.6–1.8; and it becomes higher, about 2–2.2 during the solar minimum. Our estimates of the power-law index are generally consistent with the previous results by Golub et al. (1980), 1.5–1.9, and Wolfson et al. (2000), 1.86–1.88, but significantly higher than the value of 1.19 estimated by Fisher et al. (1998). Wolfson et al. have found that at 45° and higher, the coronal emissions correlate with the lower latitude (30°) magnetic flux. Our results agree with this conclusion and provide the explanation that the correlation between the high-latitude coronal emission and the low-latitude magnetic flux is related to the giant coronal loops connecting the low-latitude active regions with the polar regions. In the axisymmetrical distributions, these loops are visible as diffuse structures extended from midlatitude to high latitude and represent impulses of coronal activity.

The connectivity between the low-latitude and polar magnetic fields, which is provided by the giant coronal loops visible in soft X-rays during the rising phase and maximum of the solar cycle and correlated with 1–1.5 yr impulses of magnetic activity, is clearly important for understanding the mechanism of the solar cycle.

This work was partly supported by the NASA JURRISS grant and the SOI/*SOHO* NASA contract NAG5-8878 to Stanford University. *SOHO* is a project of international cooperation between ESA and NASA. NSO/Kitt Peak data used here are produced cooperatively by NSF/NOAO, NASA/GSFC, and NOAA/SEL.

REFERENCES

Belvedere, G., Lanzafame, G., & Proctor, M. R. E. 1991, Nature, 350, 481
Benevolenskaya, E. E., Kosovichev, A. G., Lemen, J. R., Scherrer, P. H., & Slater, J. L. 2002, in Multiwavelength Observations of Coronal Structure and Dynamics, ed. P. C. H. Martens & D. Cauffman (New York: Elsevier), in press
Benevolenskaya, E. E., Kosovichev, A. G., & Scherrer, P. H. 2001, ApJ, 554, L107
Fisher, G. H., Longcope, D. W., Metcalf, T. R., & Pevtsov, A. A. 1998, ApJ, 508, 885
Golub, L., Maxson, C., Rosner, R., Vaiana, G. S., & Serio, S. 1980, ApJ, 238, 343
Makarov, V. I., Ruzmaikin, A. A., & Starchenko, S. V. 1987, Sol. Phys., 111, 267
Secchi, P. A. 1877, Le Soleil, Vol. 2 (Paris: Gauthier-Villars)
Sturrock, P. A. 1999, ApJ, 521, 451
Tsuneta, S., et al. 1991, Sol. Phys., 136, 37
Wolfson, R., Roald, C. B., Sturrock, P. A., & Weber, M. A. 2000, ApJ, 539, 995